https://doi.org/10.5194/egusphere-2026-3356
Preprint. Discussion started: 13 July 2026

A 10 ka ice core from Tödi (Switzerland) reveals recent surface loss and revises Alpine age–altitude relationships

Michelle M. Worek[1,2], David Wachs[3,4], Anja Eichler[1,2], Matthias Huss[5,6], Raphael Moser[5,6], Sabina Brütsch[1], Sönke Szidat[2,7], Margit Schwikowski[1,2,7], Theo M. Jenk[1,2]

[1]PSI Center for Energy and Environmental Sciences, Paul Scherrer Institute, Villigen, Switzerland
[2]Oeschger Centre for Climate Change Research, University of Bern, Bern, Switzerland
[3]Institute of Environmental Physics, Heidelberg University, Heidelberg, Germany
[4]Kirchhoff-Institute for Physics, Heidelberg University, Heidelberg, Germany
[5]Laboratory of Hydraulics, Hydrology and Glaciology, ETH Zürich, Zürich, Switzerland
[6]Swiss Federal Institute for Forest, Snow and Landscape Research, Birmensdorf, Switzerland
[7]Department of Chemistry, Biochemistry, and Pharmaceutical Sciences, University of Bern, Bern, Switzerland

Correspondence to: Theo M. Jenk (theo.jenk@psi.ch)

Abstract. Understanding whether the current decline of Alpine glaciers is unprecedented requires direct evidence of ice persistence through past warm periods. While maximum glacier extents are well constrained, for example through landmarks (moraines), minimum Holocene ice extents—particularly at high elevations—remain poorly documented. Cold, low-accumulation summit glaciers can preserve very old ice, yet these archives are increasingly threatened by recent atmospheric warming. Here we present the first ice core record from the summit glacier of Tödi at 3565 m a.s.l. (Swiss Alps). Two ice cores drilled to bedrock (~20 m) were absolute dated with multiple radionuclides (^{210}Pb, ^{3}H, ^{39}Ar, ^{14}C) complemented by glaciological observations and age–depth modelling. Based on evidence for recent surface ablation, we determined that the ice surface at the time of drilling (2023) dates to 1960 ± 1 CE. An exceptionally high-resolution radiocarbon dataset reveals stratigraphically consistent preservation of basal ice dating to ~10 ka cal BP, confirming the persistence of early Holocene ice. The Tödi basal age questions the previously suggested relationship in timing of Alpine ice-free conditions around 6 ka ago at altitudes of about 3500 m a.s.l.. Instead, our results indicate that long-term ice persistence is not controlled by elevation alone, but rather dependent on local glaciological factors. Further, our results imply that other cold-based high-altitude glaciers in the Alps may preserve older ice than currently recognized and underscore both the scientific value and increasing vulnerability of these disappearing climate archives.

1 Introduction

About 3500 glaciers exist today in the European Alps, yet models project that roughly half of their present-day volume will be lost by 2050, with up to more than 90% disappearing by 2100, depending on the CO_2 emission scenario (Zekollari et al., 2019). To assess confidence in such projections, understanding of the full range of past glacier variability, including both periods of maximum extent and intervals of minimum ice cover is beneficial, because it can provide a benchmark to constrain long-term glacier sensitivity to changes in climate conditions.

Maximum Alpine glacier extents during periods such as the Last Glacial Maximum and the Little Ice Age are well constrained by geomorphological evidence including moraines, trimlines, and cosmogenic nuclide dating (Ivy-Ochs et al., 2008; Solomina et al., 2016). In contrast, minimum ice stands during warm Holocene intervals, particularly at high elevations, remain poorly constrained, as such conditions leave little direct geomorphological imprint because they will typically be erased by subsequent advances. Subfossil wood indicates that trees colonized formerly glaciated terrain during these warm periods, providing constraints on minimum ice extents, but such evidence is largely limited to lower- and mid-elevation forefields (Le Roy et al., 2024). Numerical glacier modelling offers a framework to explore Holocene glacier evolution with reconstructed temperature and precipitation, and recent ice-flow models enable long-term, high-resolution simulations over complex Alpine terrain

https://doi.org/10.5194/egusphere-2026-3356
Preprint. Discussion started: 13 July 2026

(Jouvet et al., 2023; Karger et al., 2023; Henz et al., 2025). Nevertheless, model results for warm Holocene intervals remain weakly validated by observational data, especially above 3000 meters above sea level (m a.s.l.), thus raising the question of whether current and projected low levels of Alpine glaciation fall within the natural range of Holocene variability.

Assessing whether the ongoing decline in Alpine glaciation is historically without precedent requires climate archives, capable of recording long-term ice persistence through past warm periods and intervals of minimal glacier extent. Ice itself provides a unique archive in this regard, as it directly preserves evidence of continuous glacier presence where other proxies fail. Cold, static summit ice bodies with minimal internal deformation, termed "miniature ice caps," can preserve very old ice when frozen to bedrock and exposed to strong winds and low accumulation (Haeberli et al., 2004). However, these exceptional records are increasingly at risk of irreversible loss, as highlighted by recent melting observed above 4000 m a.s.l. on Grand Combin (Huber et al., 2024).

Building on evidence from several high-elevation Alpine summits, Bohleber et al. (2020) proposed an empirical age–altitude relationship in which the maximum age of basal ice increases systematically with elevation. This relationship has become a central framework for selecting and interpreting Alpine ice-core sites, suggesting summit altitude and the corresponding temperature as a first-order control on long-term ice preservation. Yet the physical mechanisms underlying this pattern—particularly the relative roles of elevation and local mass-balance regime—remain incompletely constrained. The summit ice cap of Weißseespitze (WSS; 3500 m a.s.l.) is a key site underpinning the age–altitude relationship (Bohleber et al., 2020). Contemporary mass-balance observations and recent ground penetrating radar (GPR) investigations indicated that WSS currently preserves only a thin ice body (around 10 m in 2019 and since decreased to less than 6 m in 2025; Wachs et al., 2026). Despite ongoing thinning and loss of its firn cover, this glacier still contains multi-millennial signals, underscoring both its importance as a reference site for long-term summit ice preservation and its sensitivity to recent atmospheric warming (Fischer et al., 2022; Spagnesi et al., 2023; Wachs et al., 2026). The Tödi massif, located in the central Swiss Alps, offers a comparable elevation summit glacier (Glarner Tödi, 3568 m a.s.l.) that allows this framework to be evaluated under different local boundary conditions.

In this study, we present results from the first ice cores drilled on Tödi using absolute dates from radionuclides complemented by glaciological observations, with ice flow, age scale, and mass balance modelling to assess ice coverage at higher altitudes during the Holocene.

2 Study Site

The Glarner Tödi ice cap is a small plateau glacier situated on the highest mountain of Canton Glarus in eastern Switzerland (Fig. 1). During the Last Glacial Maximum, the Tödi massif was fully ice-covered (Schlüchter et al., 2009), but the extent and continuity of the summit glacier during warm intervals of the Holocene remain uncertain. The glacier geometry suggests restricted horizontal ice flow and a predominance of vertical strain. The massif is characterized by exceptionally high topographic prominence (~1570 m), among the highest in Switzerland, resulting in strong wind exposure and enhanced snow redistribution. Potential permafrost distribution maps (FOEN, 2005) indicate widespread permafrost around the massif, reducing geothermal heat flow and favoring cold bedrock conditions. This raises the likelihood to find old ice frozen to bedrock, even at a relatively low elevation. Apart from a short investigation following the Chernobyl accident that examined radionuclide deposition at high altitude (Haeberli et al., 1988), no detailed glaciological study has previously been conducted on this summit glacier. Regional context is provided by long-term observations from nearby glaciers such as Biferten, Clariden, Limmern and Punteglias (GLAMOS, 2026), as well as digital elevation models (DEMs) and topographic maps indicating past surface elevation (see Section 4.3, Supplement S1; GLAMOS, 2025a; Federal Office of Topography, 1963; 1997; 2016; 2023).

https://doi.org/10.5194/egusphere-2026-3356
Preprint. Discussion started: 13 July 2026

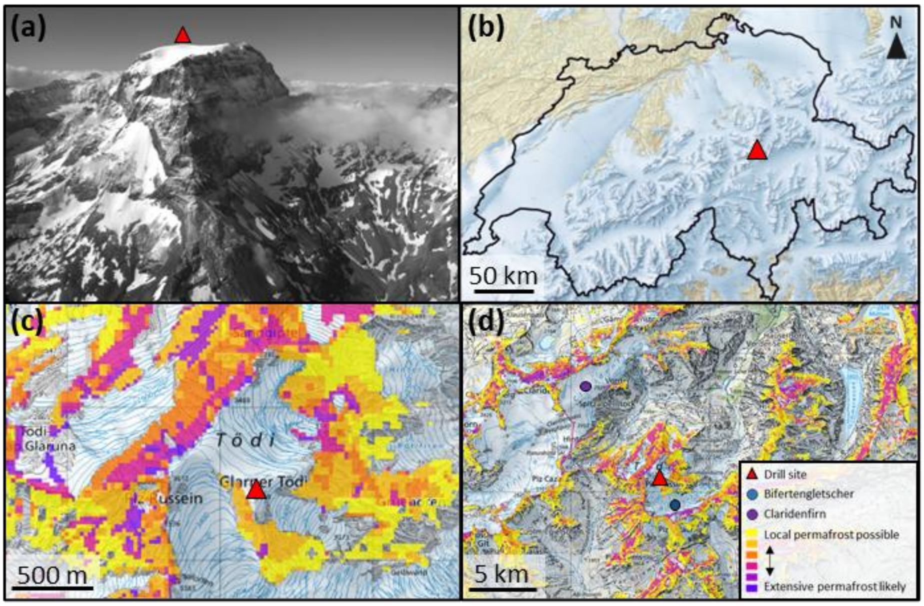

Figure 1. (a) Tödi massif as seen from north (courtesy of © Fridolin Walcher). (b) Map of Switzerland with Last Glacial Maximum ice extent (Schlüchter et al., 2009). (c) Permafrost extent of Tödi and (d) surrounding region, with present ice extent (FOEN, 2005). Glarner Tödi drill site indicated in all images with a red triangle. Bifertengletscher and Claridenfirn are also indicated in panel (d).

3 Methods

3.1 Drilling, field measurements, and core processing

Drilling was conducted on 3 to 4 May 2023 at the Glarner Tödi summit using a FELICS electromechanical drill (Ginot et al., 2002), retrieving two continuous ~20-m cores to bedrock (referred to as TÖ23-BH1 and TÖ23-BH2, Table 1). No firn was observed beneath that year's winter snow, and only pure ice was present. There is very high certainty that bedrock was reached. In TÖ23-BH1, a 72 cm long, intact ice core segment was recovered, showing a clean break with no inclusions of potential silt or small rocks from the bed, as often observed from other Alpine ice cores. In the subsequent run, the drill head hit the bed after 11 cm of penetration, evidenced by strong vibrations transmitted along the cable, a distinguished noise from grinding against a hard surface, and visible damage on the cutters. No break was required before lifting the drill, and a short and completely intact piece of clean ice (11 cm) was recovered. The bottom surface of that segment was smooth, with a fine imprint throughout the cross section, likely from the surface of the glacier bed (see Supplement S2). Similar conditions were experienced for the parallel core, TÖ23-BH2. In addition to the two long cores, a third shallow core (3 m) and several short surface cores were drilled for the availability of sufficient ice mass for argon-39 (^{39}Ar) dating. All short cores were drilled within ~1 m of TÖ23-BH1 and TÖ23-BH2.

In addition, GPR profiles were collected along and across the summit using a 250 MHz antenna. At the same time, winter snow depth was measured at 44 positions based on manual probing down to the clearly defined last summer horizon (see Supplement S3). The measurements were spread over the top part of the Tödi ice cap and used to assess winter snow accumulation distribution. A thermistor chain equipped with sensors spaced every 0.5 m and calibrated over a range of −25 to 25 °C was installed overnight in TÖ23-BH1 for in-situ englacial temperature measurements, allowing sufficient time to reach

https://doi.org/10.5194/egusphere-2026-3356
Preprint. Discussion started: 13 July 2026

equilibrium. At each sensor, a stack of continuous temperature measurements was acquired over time and combined to produce the final temperature record.

Table 1. Borehole descriptions from 2023 drilling campaign on Tödi. Coordinates refer to Switzerland's official satellite-based geodetic reference frame (LV95). Core numbers correspond to individually drilled core sections (used in ^{14}C sample names).

Borehole	Drilling Date	Elevation (m a.s.l.)	Latitude (LV95)	Longitude (LV95)	Depth (m)	Core Numbers
TÖ23-BH1	03.05.2023	3566	1185447	2713210	19.85	6-35
TÖ23-BH2	04.05.2023	3565	1185449	2713209	19.76	36-68

Core segments, each approximately 70 cm in length (8.2 cm in diameter), were logged and packed in polyethylene tubes, placed in insulated boxes for transport and storage at -20 °C at the Paul Scherrer Institute (PSI). The core quality was excellent throughout, from surface to bedrock, with very few unintended breaks. Unless otherwise stated, all discrete samples for analyses were taken from the TÖ23-BH2 core. Most of the parallel TÖ23-BH1 core could thus be preserved intact for potential replicate measurements and future analyses.

All ice core processing and subsampling took place in the PSI cold room (-20 °C) under well-established clean procedures as described in Eichler et al. (2000). The focus of this study was achieving the highest possible resolution for ^{14}C dating of the ice core. Therefore, most ice was reserved for ^{14}C dating with the aim of utilizing the least amount of ice required for analysis and optimized for reasonably low uncertainty which is constrained by the carbon mass that can be extracted per sample (Dyonisius and Jenk, 2025). With this strategy, ^{14}C samples varied in depth resolution (see Section 4.4). All samples were from the TÖ23-BH2 core except for samples Tö23-34.1 and Tö23-34.2, where additional ice from the TÖ23-BH1 core was sampled, and Tö23-68_34_35, which combines ice from both TÖ23-BH1 and TÖ23-BH2. These three additional samples were incorporated to increase the dating resolution of basal ice. Depth alignment for this section was narrowly constrained by the bedrock. ^{14}C samples were packed in pre-washed polyethylene terephthalate glycol (PETG) jars (1000 mL, Semadeni), which were rinsed three times, then filled with ultrapure water and left to soak overnight; this cleaning cycle was repeated five times. Samples for lead-210 (^{210}Pb) were cut continuously from 0 to 5.2 m depth, each approximately 60 cm in length. Tritium (^{3}H) samples were cut from 0 to 5.2 m depth, each approximately 20 cm in length. Both ^{210}Pb and ^{3}H samples were packed in pre-rinsed PETG jars. Samples for refractory black carbon (rBC) were cut continuously at 1.8 cm resolution from the surface to approximately 12 m depth. To maximize ice availability for ^{14}C sampling, resolution was reduced to 3 cm from 12 m depth to the bottom of the core. Samples were placed in pre-washed (same cleaning procedure as described for ^{14}C) polypropylene (PP) vials (50 mL, Sarstedt). The sampling strategy was adapted depending on the sensitivity of the analysis to contamination. For ^{14}C and rBC, samples were taken from the inner part of the core (minimum 3 mm removed from outer layer) to minimize contamination from all core handling. Samples for ^{210}Pb and ^{3}H analyses, less sensitive to external contamination, were cut from the outer portion of the core. For ^{39}Ar, several short cores were collected to achieve sufficient gas concentration and shipped frozen to the Institute of Environmental Physics and Kirchhoff-Institute for Physics (Heidelberg, Germany) for analysis.

3.2 ^{210}Pb, ^{3}H, ^{39}Ar and rBC analysis

With a half-life of 22.3 years, ^{210}Pb allows dating of ice up to around 150 years, depending on the initial activity concentration deposited on the glacier surface (Gäggeler et al., 2020). ^{210}Pb was analysed in samples of around 200 mL, using α-counting of its grand-daughter ^{210}Po (5.3 MeV α-line), following the established method and approach for dating glacier ice (Gäggeler et al., 1983; Gäggeler et al., 2020). The analytical background was 1.1 mBq kg^{-1} and the contribution from supported Pb (produced in situ from the decay of mineral dust-incorporated radionuclides) 2.6 ± 0.3 mBq kg^{-1} (see Supplement S4).

https://doi.org/10.5194/egusphere-2026-3356
Preprint. Discussion started: 13 July 2026

^3H (half-life of 12.3 years) allows detection of the signal from the extensive atmospheric (surface) nuclear-weapons testing in the 1960s, with potential for identification of the distinct 1963 CE atmospheric peak (partial test ban treaty thereafter) which can serve as a robust time marker in glacier ice (Schotterer et al., 1998). ^3H analysis was performed on 10 mL aliquots of melted ice samples, 1:1 mixed with a scintillation cocktail (Ultima Gold LLT), at PSI using low-level scintillation counting (liquid scintillation counter: TriCarb 2770 SLL/BGO, Packard SA). The total count time was 1500 min with an analytical detection limit of 0.12 Bq kg^{-1}.

With a half-life of 268 ± 8 years (Chen, 2018), ^{39}Ar allows dating of argon gas trapped in the air bubbles in the ice for the age range from around 50 to 1800 years (Ritterbusch et al., 2022). ^{39}Ar, quantified as an isotopic abundance ($^{39}Ar/Ar$), was prepared at the Institute of Environmental Physics and measured using Atom Trap Trace Analysis (ATTA) at the Kirchhoff-Institute for Physics following the methods described in Wachs et al. (2026). The results are expressed in percent modern argon (pmAr), defined as the sample abundance normalized to the modern atmospheric reference value (R_a).

rBC concentrations were analysed using a single-particle soot photometer (SP2), following the procedures and method described in Wendl et al. (2014), adopting the improvements related to automatization and correction for wall absorption effects later introduced by Osmont et al. (2018).

3.3 Radiocarbon (^{14}C) analysis

^{14}C analyses targeted the water-insoluble organic carbon (WIOC) fraction entrapped in the ice. This approach is well established for dating ice cores where conventional layer counting is not possible (Jenk et al., 2007; Uglietti et al., 2016; Preunkert et al., 2019; Fang et al., 2021; Hou et al., 2025). Samples were processed following the method described in Uglietti et al. (2016). In brief, melted ice samples were filtered through pre-combusted quartz-fibre filters to isolate WIOC, then acidified with hydrochloric acid (HCl) for the removal of carbonates (here following the improved procedure for higher removal efficiency described in Hou et al. 2025), and WIOC subsequently combusted using a Sunset OC/EC analyzer equipped to a gas interface system (GIS) for accelerator mass spectrometry (AMS) analysis (Agrios et al., 2015).

^{14}C measurements were performed at the Laboratory for the Analysis of Radiocarbon with AMS, University of Bern, using the Mini Carbon Dating System (MICADAS) instrument (Synal et al., 2007; Szidat et al., 2014). All results are reported as fraction modern ($F^{14}C$), which is the ratio of $^{14}C/^{12}C$ in the sample relative to that of the modern reference standard, normalized to the year 1950 CE. The reference material used was oxalic acid II (National Institute of Standards and Technology (NIST), SRM 4990C) with both samples and standards corrected for isotopic fractionation ($\delta^{13}C$ normalization to -25‰). Ice samples were calibrated using a modern reference (NIST oxalic acid II, SRM 4990 C; $F^{14}C$ of 1.3407 ± 0.0005) and fossil reference (sodium acetate, Sigma-Aldrich, no. 71180; $F^{14}C$ of 0.0018 ± 0.0005). ^{14}C results were first corrected for cross contamination (0.5% $F^{14}C$ carryover from the preceding sample) and for constant contamination from the AMS system background (0.4 ± 0.2 µg C with $F^{14}C$ of 0.8 ± 0.4; Agrios et al., 2015; Uglietti et al., 2016). A procedural blank correction was then applied treating frozen blocks of ultra-pure water as glacier ice samples, with values as reported in Fang et al. (2021) of 1.3 ± 0.6 µg C with $F^{14}C$ of 0.69 ± 0.15. Finally, ^{14}C results were calibrated using OxCal v4.4.4 (Ramsey, 1995; 2021) with the IntCal20 calibration curve (Reimer et al., 2020) and the OxCal built-in Bayesian sequence model (P_Sequence, accounting for knowledge about increasing age with depth; Ramsey, 2008; 2009). Calibrated ^{14}C ages are expressed in years before present (cal BP = 1950 CE) unless stated otherwise, with uncertainties indicating the 1σ range.

For the comparison of the calibrated Tödi ^{14}C ages with other Alpine ice core records (see Section 4.5), ages were plotted as years before 2000 CE (years b2k; Rasmussen et al., 2006) and referenced to height above bedrock (m w.e.) for consistency independent of glacier thickness or surface age at time of drilling. Where reported ages correspond to depth intervals, depths are assigned to the midpoint of the interval. For this comparison, all calibrated ^{14}C dates indicate the µ-age (the probability-weighted mean of the calibrated age probability distribution function provided by OxCal) with 1σ uncertainty. For studies

https://doi.org/10.5194/egusphere-2026-3356
Preprint. Discussion started: 13 July 2026

where µ-ages were not explicitly reported as such, ages were re-calibrated in OxCal from the available $F^{14}C$ data or provided radiocarbon ages to ensure consistency in calibration and uncertainty estimation across sites.

3.4 Ice flow, age scale and mass balance models

To better understand the past conditions of the study site, the ice flow dynamics resulting in the vertical strain of the ice, and to ultimately construct a continuous age–depth relationship for the Tödi ice core, complementary models were applied: the one-dimensional ice flow model from Dansgaard-Johnsen (D-J, Dansgaard and Johnsen, 1969), based on the physics of plastic deformation caused by viscous flow and consequential stress but for the assumption of steady-state conditions, and the COPRA model which is a purely statistical model only based on age probabilities, and accordingly not constrained/restricted by any physical assumptions (Breitenbach et al., 2012). The D–J model parameter estimates can be constrained by ages of dated layers in the ice core (see Section 4.4, see Supplement S5 for model details and fitting procedure). Both the D–J model and the COPRA model have been applied and investigated in previous studies on alpine ice cores (e.g., Fang et al., 2023; Hou et al., 2025; Gabrielli et al., 2026).

To satisfy the underlying physics of the ice-flow models (the incompressibility of ice, in contrast to the compressibility of firn by densification), depth and ice thickness were converted from meter to meter water equivalent (m w.e.; depth times density), with accumulation rates expressed in m w.e. a^{-1}. Thereby the density of 910 kg m^{-3} was derived from the measured density ranging between around 900 to 920 kg m^{-3}. Thus, depth is expressed in units of either m or m w.e.; the total TÖ23-BH2 core length is 19.76 m, corresponding to 17.98 m w.e.. To assess the past ice thickness H and accounting for the potential presence of firn at that time (see Section 4.3), the D-J model was coupled to the classical firn densification model by Herron and Langway (1980) with an optimized empirical factorization specifically for alpine sites (Huss, 2013). See details in Supplement S5.

The COPRA model allows constructing an ensemble of Monte Carlo age–depth realizations consistent with the input of dated horizons, their uncertainties, and stratigraphic ordering (Markov chain Monte Carlo simulation, here based on 2000 simulation runs; Breitenbach et al., 2012). Median ages and confidence intervals were derived from the resulting ensemble, providing an age-depth relationship with an associated uncertainty.

For interpreting the temporal dynamics and spatial variability of surface mass balance over the Tödi ice cap we applied a distributed accumulation and temperature-index melt model (Huss et al., 2021). Long-term homogenized daily temperature and precipitation data from the Säntis weather station (2501 m a.s.l., 58 km from the study site) since 1884, and between 1864 and 1884 from Sils (76 km from the site) were extrapolated to Tödi and used to compute spatial mass balance distribution over the entire summit glacier at 10 m resolution. Snow accumulation totals and their variability in space were constrained using the snow depths surveys in May 2023 (see Section 3.1). We used the observed ice volume change 2013-2022 of the entire glacier (GLAMOS, 2025a) in connection with an assumption on frontal ice-avalanche losses to constrain the ablation component of the model. Long-term model runs 1864-2025 provide gridded surface accumulation rates and may thus indicate periods dominated by accumulation or ablation at a local scale.

Snow accumulation on high-elevation summit ice caps is strongly determined by the air temperature during snow fall (Guillet and Ravanel, 2020; Eidevåg et al., 2022). Snow at very cold temperatures is dry and light, thus preferentially relocated by wind and deposited at more protected locations, leading to spatial and temporal mass balance variability. This is indicated by the spatial snow depth distribution observed in May 2023 where the drill site was almost snow-free while snow depths of up to 4 meters were found lower down (see Supplement S3). Snow accumulation in these topographic situations often happens only at air temperatures above ca. −5 °C (Guillet and Ravanel, 2020). We therefore implemented a corresponding temperature-dependent accumulation correction in the mass balance model. This approach accounts for the asymmetry of snow accumulation by prescribing zero snow accumulation below −8 °C with linearly decreasing accumulation from −4 to −8 °C.

https://doi.org/10.5194/egusphere-2026-3356
Preprint. Discussion started: 13 July 2026

4 Results and Discussion

4.1 Ground penetrating radar and ice temperature

GPR surveys conducted around the drill site on the Glarner Tödi summit provide detailed constraints on glacier geometry. An extensive grid of profiles shows an ice thickness of approximately 20 m at the drilling location, in close agreement with the ice core length, with maximum thickness reaching up to ~40 m in other parts of the summit glacier (Fig. 2a-b). GPR profiles 24 and 43 intersecting the drill site reveal a low-angle bedrock topography beneath the ice cap (Fig. 2c, see Supplement S3). These results indicate that the ice cores were drilled at a location of low ice flow and limited driving stress, which favors undisturbed stratigraphic layering.

Englacial temperatures show that the Tödi summit ice cap remains frozen to bedrock (Fig. 2d). Temperature near the ice–bedrock interface is approximately −4 °C. The lower temperatures observed in the upper part of the borehole reflect near-surface conditions at the end of winter and ambient air temperatures. Air temperatures around −8 °C are consistent with mean annual air temperatures reported from other high elevation sites, including WSS (Fischer et al., 2022), Jungfraujoch (Leuenberger and Flückiger, 2008) and Ortles (Carturan et al., 2023). The increase in englacial temperature with depth is likely driven by geothermal heat flux from the bed.

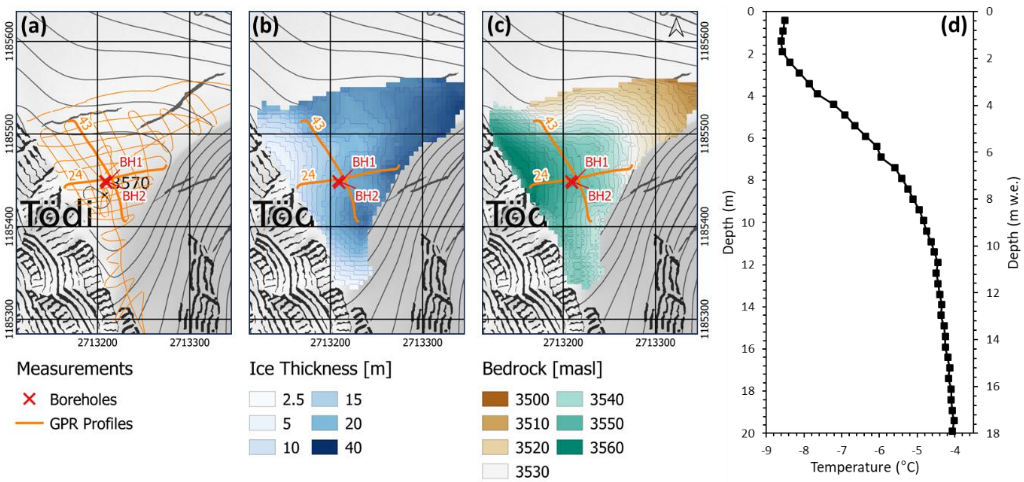

Figure 2. (a) GPR profiles covering the drill site area, boreholes indicated with red x (see Supplement S3 for profiles 24 and 43). Maps of (b) ice thickness and (c) bedrock topography, resolved from GPR. (d) Temperature profile in TÖ23-BH1, against depth in m (left y-axis) and m w.e. (right y-axis).

4.2 Dating of the near surface ice

Due to the observed absence of firn, the assumption that the surface ice age corresponds to the drilling year is no longer valid. This situation poses a fundamental challenge for establishing a reliable ice-core chronology. Independent age constraints were therefore established.

^{210}Pb activity concentrations decrease with depth, corresponding to an increase in age with respect to the surface (Fig. 3). However, the derived surface activity of approximately 25 mBq kg^{-1} is substantially lower than 90 ± 20 mBq kg^{-1} reported for other sites in the European Alps (Gäggeler et al., 2020), suggesting progressed radioactive decay and indicating an older surface age (1983 ± 20 CE). Since the few ^{210}Pb data points cover only part of the theoretically datable 150 years, the uncertainty is large and accuracy is limited. The results from ^{3}H analysis can narrow this surface constraint. Here, we compare

https://doi.org/10.5194/egusphere-2026-3356
Preprint. Discussion started: 13 July 2026

^3H concentrations from Tödi (measured in 2023) with expected ^3H levels based on concentrations from another Alpine ice core (Grenzgletscher), where Eichler et al. (2000) showed the presence of the distinct ^3H peak, corresponding to 1963 from nuclear bomb testing, preceded by low pre-bomb concentrations and followed by depleted post-bomb levels (Fig. 4a). At Grenzgletscher, the ^3H activity concentration reached up to 100 Bq kg^{-1} for the 1963 layer, as determined for the time of drilling in 1994 (Eichler et al., 2000). Averaged over the period 1960–1965 to match the approximate temporal resolution of the Tödi samples (~5 years, based on the initial ^{210}Pb estimate), this results to ~25 Bq kg^{-1}. Accounting for the radioactive decay of ^3H since 1994, the ^3H activity concentration in the 1960-1965 layer is expected to be ~5 Bq kg^{-1} at present (i.e., at the time of the Tödi sample analyses in 2023). Similarly, the expected levels for post- and pre-nuclear testing periods (1965-1970 and 1955-1960, respectively) are ~2.5 and ~0.3 Bq kg^{-1}, respectively. We measured ^3H concentrations near the detection limit (0.12 Bq kg^{-1}), consistent with pre-1960 levels, and no bomb peak was detected (Fig. 4b), indicating a surface age older than ~1960.

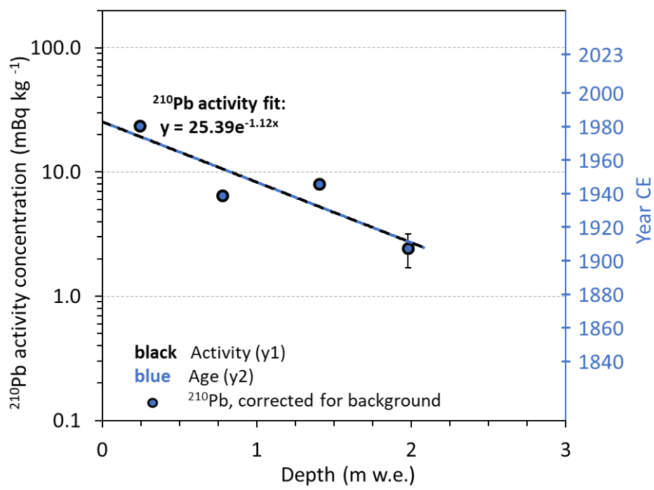

Figure 3. ^{210}Pb activity concentration (black, left y-axis) as a function of depth in m w.e., with corresponding age in years CE (blue, right y-axis). The intercept of the linear regression of ln(^{210}Pb activity), dashed black line, yields the ^{210}Pb activity surface concentration. By applying the law of radioactive decay under the assumption of constant initial deposition (90 mBq kg^{-1}, see Gäggeler et al., 2020) the corresponding age was derived (blue dashed line, right y-axis).

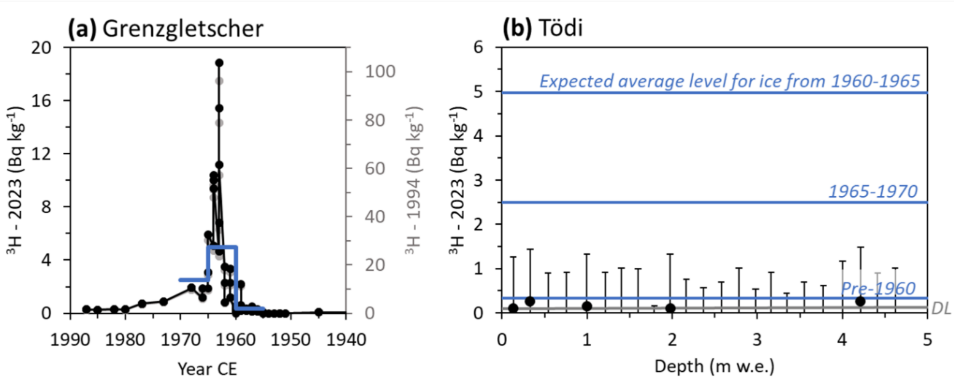

Figure 4. (a) ^3H concentrations from Grenzgletscher measured in 1994 (gray, right y-axis) (Eichler et al., 2000), and here accounting for decay until 2023 (black, left y-axis), with five-year averages indicated in blue. (b) ^3H concentrations from Tödi measured in 2023, with most

https://doi.org/10.5194/egusphere-2026-3356
Preprint. Discussion started: 13 July 2026

values close to the detection limit (DL, gray line). For values below the DL, only error bars are shown. Expected concentrations for the specified time periods based on the Grenzgletscher averages (considering decay until 2023) are indicated as a reference (blue lines).

Additional age constraints were derived from comparing rBC concentrations with the rBC record from Colle Gnifetti (CG; Sigl et al., 2018) and elemental carbon (EC) record from Fiescherhorn (FH; Jenk et al., 2006; Fig. 5). A several-fold increase in rBC concentrations is observed at 4.8 m w.e., from <1 µg L^{-1} to ~6 µg L^{-1} (0.5 m w.e. averaged concentrations) (Fig. 5a). This trend is consistent with rBC CG and EC FH decadal averages (Fig. 5b), where Sigl et al. (2018) identified the time of emergence from pre-industrial to industrial levels at 1875 ± 8 CE. We used this feature at a depth of 4.8 m w.e. as an additional age tie-point (1875 CE, with a slightly more conservative uncertainty of ± 10 years).

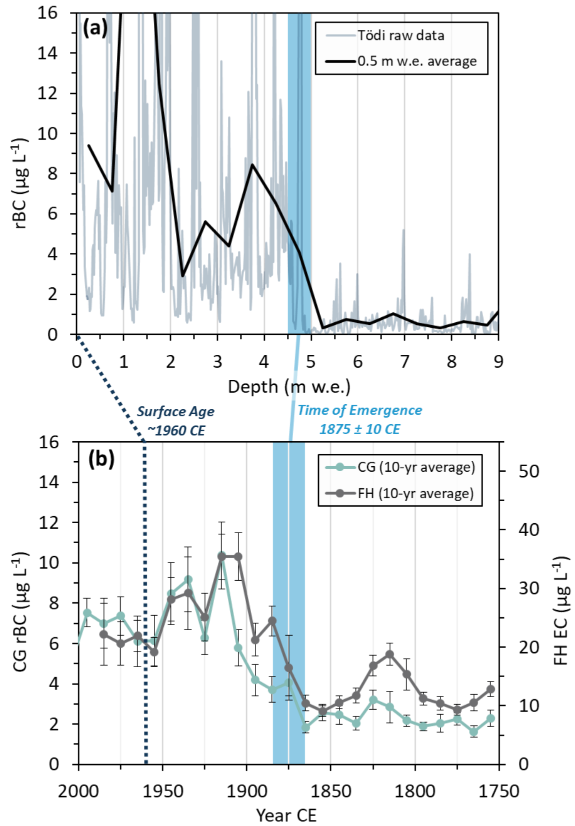

Figure 5. (a) rBC concentrations from Tödi for 0 to 9 m w.e., with 0.5 m w.e. averages. (b) Colle Gnifetti (CG) rBC and Fiescherhorn (FH) EC 10-year averages from 1750 to 2000 CE (Jenk et al., 2006; Sigl et al., 2018). Time of Emergence (1875 ± 10 CE) indicated in blue band, corresponding with rBC increase in Tödi. Tödi surface age estimate (~1960 CE) marked in dashed line.

From the two samples analysed for ^{39}Ar (Table 2), only Tö23-Ar2 yielded sufficient Ar volume for a reliable age of the ice of 114^{+77}_{-72} years at 2.4 m w.e., although with a high uncertainty. The low Ar content in Tö23-Ar1 from 0.2 m w.e. depth might be related to melt effects in the weather crust at the surface. Large uncertainty here is also due to the dilution factor from mixing the sample with ^{39}Ar-free argon for sufficient measurement volume. To account for the difference in age between ice and gas, we applied a correction of 18 ± 12 years for the delta age (Δage, see Supplement S6).

https://doi.org/10.5194/egusphere-2026-3356
Preprint. Discussion started: 13 July 2026

Table 2. Sample details and results of ^{39}Ar dating. Ages are in years before 2023. The age in brackets was not further considered because of low Ar sample volume. The ice age includes a correction for the gas-ice age difference (Δage).

Sample	Mid-depth (m w.e.)	Sample mass (kg)	Extracted air volume (mL)	Extracted Ar volume (mL)	pmAr	Ar gas age (years)	Ice age (years)
Tö23-Ar1	0.19	5.0	52.2	0.23	0.61	(189^{+211}_{-142})	-
Tö23-Ar2	2.42	2.9	65.0	1.3	0.78	96^{+65}_{-60}	114^{+77}_{-72}

4.3 Determination of the ice surface age, recent surface loss and variations in mass balance

By combining the dating based on ^{210}Pb, ^{3}H, ^{39}Ar, and rBC (see Section 4.2), the surface age of the ice in 2023 could finally be determined. This was achieved through fitting the D-J model (accounting for layer thinning) to the data, with the fit backward extrapolated to the expected initial ^{210}Pb surface activity concentration (90 ± 20 mBq kg^{-1}), providing us with an estimate of the ice surface age in 2023 equal to 1960 ± 1 CE and a surface loss (ablation) since 1960 of 5.6 ± 1 m w.e., corresponding to ~8.1 m (Fig. 6). We further derive the corresponding average ice thickness for this period (1960-2023) as the 2023 ice thickness (17.98 m w.e., 19.76 m) plus the net ablation, yielding 23.6 ± 1 m w.e. (~27.9 m).

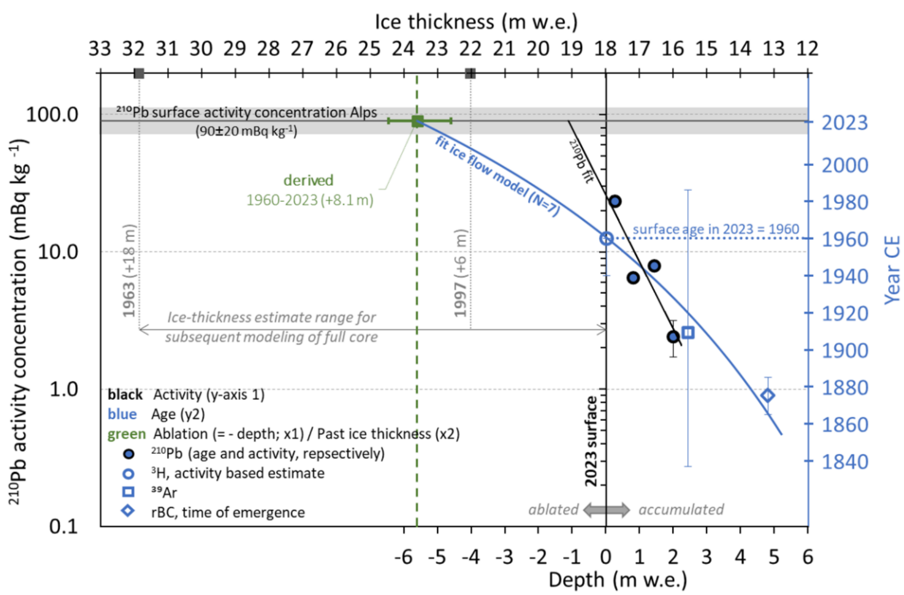

Figure 6. ^{210}Pb activity concentrations (left y-axis) and related age (right y-axis), with additional dating results from ^{3}H, ^{39}Ar, and rBC (see Section 4.2). Fit to ^{210}Pb data only (black line; same as in Fig. 3) and fit to all data points by the D-J model (blue line) for a best estimate of the ice surface age in 2023 (intercept at depth = 0 m w.e.). Backward extrapolation of the fits to the expected initial ^{210}Pb surface activity concentration (90 ± 20 mBq kg^{-1}, gray line with band) yields the ablation since 1960 (lower x-axis) and the past (average) ice thickness from 1960-2023 (upper x-axis), green square and vertical line. Reference ice thicknesses (gray squares) based on topographic maps are shown in addition as a range of past variation (see Fig. 7). For the conversion from m to m w.e., the presence of a firn column was assumed with the density profile derived from the density model (see Section 3.4).

To place this derived surface loss in a broader regional framework, cumulative mass balance of Claridenfirn (GLAMOS, 2025b) and recent surface elevation changes of Glarner Tödi based on DEMs (GLAMOS, 2025a) and topographic maps

https://doi.org/10.5194/egusphere-2026-3356
Preprint. Discussion started: 13 July 2026

(Federal Office of Topography, 1963, 1997, 2016, 2023) were compared (Fig. 7). Elevation data for Glarner Tödi are limited, but as shown in Figure 7a, a decrease over the past decades is evident, with the 2023 summit elevation 8.4 m lower than the map based mean elevation for the 1963-2023 period (3576.4 m a.s.l.), in excellent agreement with our derived average ice thickness lowering of 8.1 m for nearly the same period (1960-2023). Long-term mass balance records at Claridenfirn (Fig. 7b) showed relatively stable conditions until approximately the 1990s, followed by a pronounced decline toward the present (Huss et al., 2021). There is evidence that firn was still present on Tödi in 1986, as indicated by the shallow (2–3 m) firn core sampled for Chernobyl fallout (Haeberli et al., 1988). Also, a local mountain guide who has climbed Tödi more than 400 times since 1974 reported that first significant changes in firn conditions began in the past 15-20 years and have accelerated, particularly over the last five years; he also noted retreat of the southwest rim of the small ice cap near the drilling site (pers. communication H. Rauner, 2023). Together, these observations indicate substantial glacier thinning and mass loss in the region over the past several decades, with increasing severity and rate since around the year 2000.

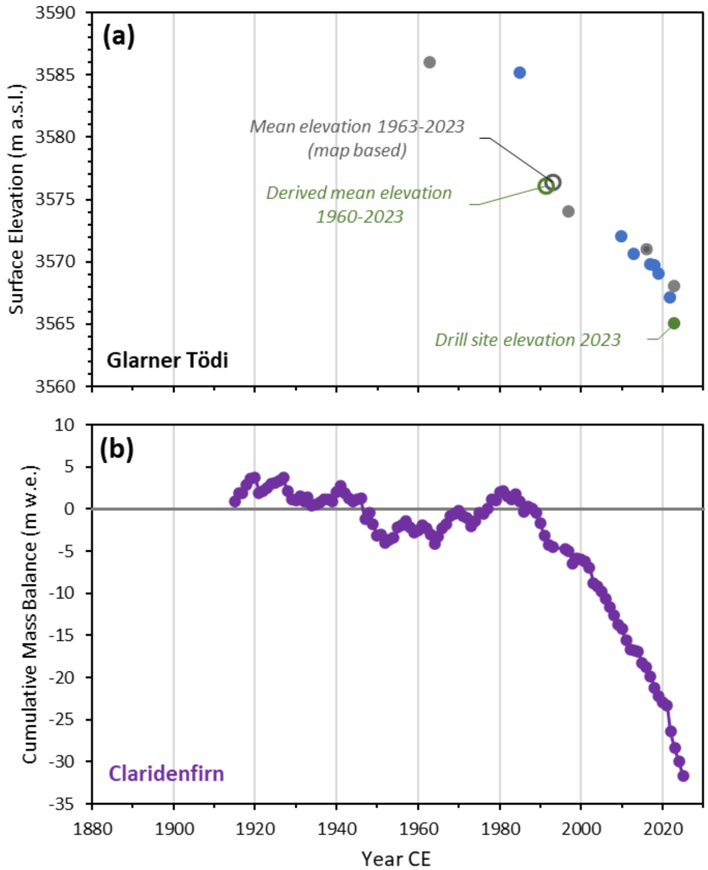

Figure 7. (a) Glarner Tödi surface elevation from DEMs (blue points) and topographic maps (gray points) with the mean elevations based on the topographic maps (1963-2023, gray open circle) and derived from surface and near-surface dating (1960-2023, green open circle; see Fig. 6). Note, map elevations are indicative for the summit (local maximum elevation) with slightly varying coordinates in time and a few meters offset from the drill site elevation in 2023 (green). Also, the year of map production may slightly differ from the year of measurement acquisition. The DEM data were extracted for the coordinates of the drill site. (b) Cumulative mass balance of Claridenfirn (period 1914-2025). Elevation and mass balance data from Federal Office of Topography (1963, 1997, 2016, 2023); GLAMOS (2025a, 2025b).

https://doi.org/10.5194/egusphere-2026-3356
Preprint. Discussion started: 13 July 2026

For further insight into these temporal variations, cumulative point surface mass balance was modelled based on the distributed accumulation and temperature-index melt model forced with temperature and precipitation data (see Section 3.4). Annual accumulation and ablation rates for the drill location over the time period 1875-2025 were extracted. Results correspond to surface processes only and cannot be interpreted as net surface elevation changes, as ice flow processes are not incorporated in the modelling approach. Local annual surface mass balances are represented cumulatively. As the model cannot be expected to resolve the exact spatial distribution of snow accumulation and ablation processes on the Tödi summit ice cap, we applied a debiasing step of the cumulative point mass balance at the drill location by enforcing a surface age of 1960, as inferred from the ice core analysis (Fig. 6). This is achieved by applying a constant local mass balance offset to the whole series that achieves a cumulative mass balance equal to zero between 1960 and 2023. This is done both for the mass balance model version with standard snow accumulation, and the version with reduced accumulation for very low air temperatures as shown in Figure 8 (see Section 3.4). We find that both confirm the total ice loss on Tödi up to the drill date in 2023 of around 6 m w.e., as independently determined based on the ice core data (Fig. 6). The model results indicate that net accumulation stopped around 1980 but sustained firn and ice loss only started in 2015 with rapidly increasing rates up to 2025, as also documented by direct annual observations on nearby glaciers and consistent with H. Rauner's observations on Tödi (Fig. 7, GLAMOS, 2026). Between 1875-1960, accumulation was consistent except for a short interruption in the 1940s (see e.g. Huss et al., 2009). Average accumulation rates are significantly lower (0.28 m w.e. a^{-1}) for the model version at low temperature, accounting for lower snow deposition due to higher wind erosion (Fig. 8).

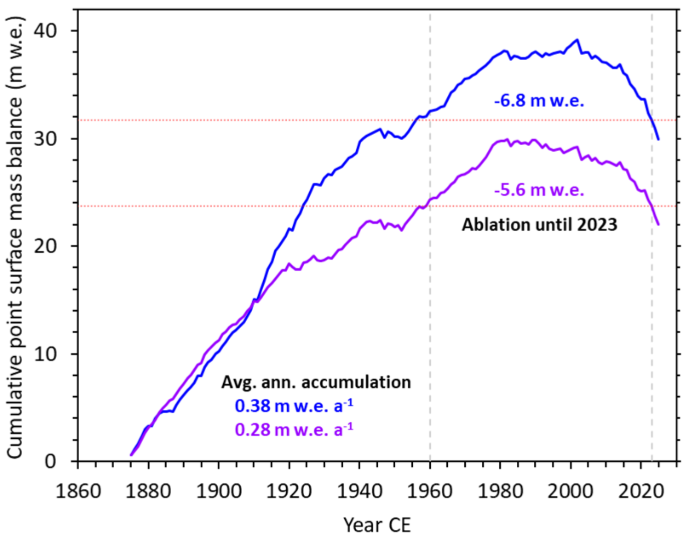

Figure. 8. Modelled cumulative annual mass balance at the drill location, calibrated to match the dated surface of 1960, for the standard model (blue) and the model version accounting for reduced snow precipitation at very low air temperatures (purple). The total modelled ablation between the 1980s until 2023, as well as the average accumulation rate between 1875 and 1960 is given.

4.4 Radiocarbon dating and age-depth modelling

The calibrated ^{14}C dates result in a high-resolution chronology of consistent stratigraphic order (Table 3), with an age of the deepest ice at 17.89 m w.e. (0-21 cm above bedrock) of 9967 ± 367 cal BP. As described in Section 3.3, ages were calibrated with the OxCal in-built P_Sequence model (Fig. 9). Although this has little effect on the so derived mean or median ages compared to the initial results, it is still beneficial because of generally reduced uncertainties (i.e., smaller probability range)

https://doi.org/10.5194/egusphere-2026-3356
Preprint. Discussion started: 13 July 2026

in particular for samples of younger age (less than around 500 cal BP where the atmospheric calibration curve is relatively flat) and/or individual samples of lower analytical precision (e.g. Tö23-62). The resulting posterior distributions define the most probable calibrated age–depth relationship to bedrock for the Tödi ice core.

Table 3. ^{14}C samples from Tödi ice core, used in the age model. F^{14}C-AMS refers to raw results. F^{14}C-corrected indicates results after background and blank corrections (see Section 3.3). Cal BP refers to calibrated years before 1950. Uncertainties reflect 1σ confidence intervals.

Sample Name	AMS Lab ID	Depth (m w.e.)	Ice mass (kg)	Carbon mass (μg C)	F^{14}C-AMS	F^{14}C-corrected	^{14}C age (yr BP)	Calibrated ^{14}C age (cal BP, 1σ range)	μ age (cal BP)
Tö23-53	23281.1.1	9.20 – 9.85	0.553	68.1	0.960 ± 0.008	0.967 ± 0.009	271 ± 78	146-338	257 ± 85
Tö23-54	23282.1.1	9.85 – 10.49	0.488	61	0.942 ± 0.008	0.947 ± 0.010	434 ± 82	310-397	370 ± 51
Tö23-56	23412.1.1	10.89 – 11.54	0.358	25.7	0.939 ± 0.007	0.957 ± 0.016	355 ± 133	369-480	421 ± 51
Tö23-58	23413.1.1	12.15 – 12.65	0.501	47.2	0.946 ± 0.007	0.954 ± 0.010	380 ± 84	442-523	474 ± 45
Tö23-60	23498.1.1	13.20 – 13.80	0.452	68.2	0.931 ± 0.008	0.935 ± 0.009	537 ± 77	515-634	575 ± 47
Tö23-61	23499.1.1	13.80 – 14.47	0.408	79.5	0.894 ± 0.008	0.897 ± 0.009	874 ± 78	680-805	771 ± 66
Tö23-62	23500.1.1	14.47 – 14.97	0.390	14.6	0.871 ± 0.009	0.889 ± 0.025	944 ± 228	786-978	897 ± 94
Tö23-63	23501.1.1	14.97 – 15.62	0.455	45.6	0.866 ± 0.008	0.872 ± 0.010	1102 ± 90	937-1118	1038 ± 85
Tö23-64	23502.1.1	15.62 – 16.02	0.371	38.8	0.847 ± 0.008	0.853 ± 0.010	1282 ± 97	1128-1295	1200 ± 80
Tö23-65	23503.1.1	16.02 – 16.44	0.466	123	0.824 ± 0.008	0.825 ± 0.009	1544 ± 86	1357-1520	1445 ± 83
Tö23-65_66	23504.1.1	16.44 – 16.85	0.460	111.4	0.764 ± 0.008	0.765 ± 0.009	2153 ± 91	2004-2305	2410 ± 123
Tö23-66	23505.1.1	16.85 – 17.30	0.448	90	0.697 ± 0.007	0.699 ± 0.008	2882 ± 90	2880-3145	3023 ± 124
Tö23-34.1	23696.1.1	17.24 – 17.46	0.189	103.4	0.614 ± 0.006	0.615 ± 0.008	3909 ± 99	4156-4511	4333 ± 158
Tö23-67.1	23506.1.1	17.30 – 17.74	0.583	149.4	0.498 ± 0.006	0.498 ± 0.007	5598 ± 115	6285-6529	6407 ± 123
Tö23-34.2	23697.1.1	17.47 – 17.70	0.180	37.9	0.455 ± 0.005	0.444 ± 0.009	6521 ± 156	7273-7569	7407 ± 154
Tö23-67.2	23700.1.1	17.74 – 17.79	0.129	394.3	0.353 ± 0.004	0.356 ± 0.007	8301 ± 158	9035-9451	9237 ± 187
Tö23-68_34_35	23507.1.1	17.79 – 17.98	0.378	27.2	0.355 ± 0.005	0.334 ± 0.013	8817 ± 323	9542-10227	9967 ± 367

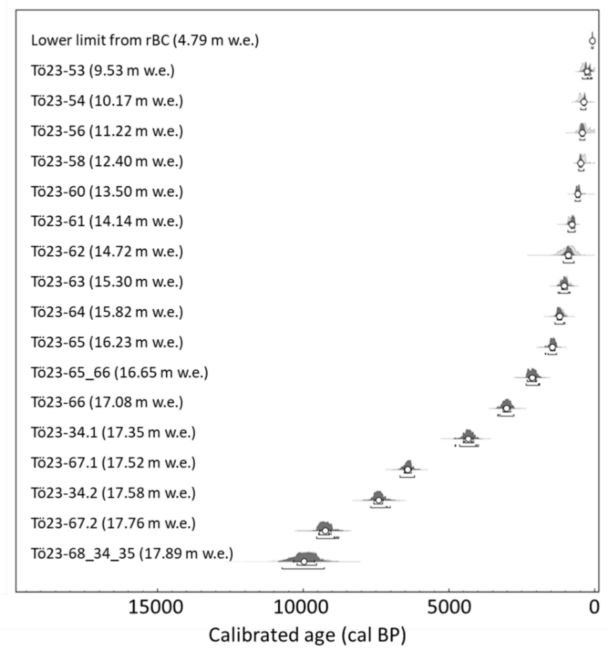

Figure 9. Radiocarbon samples listed in stratigraphic order from top to bottom for P_Sequence calibration in OxCal v4.4.4 (Ramsey, 2021) with IntCal20 curve (Reimer et al., 2020). For the individual samples (provided with mid-depth), the probability distribution functions (PDFs) indicate calibration without constraint from stratigraphic order (light gray) and when applying P_Sequence (dark gray). The bars

https://doi.org/10.5194/egusphere-2026-3356
Preprint. Discussion started: 13 July 2026

below the PDFs indicate the 1σ and 2σ range, respectively, and the open dots the μ-age (probability weighted mean age) with the 1σ uncertainty bar. For the sequence calibration, the lower age limit is constrained by the near-surface dating (rBC tie-point, see Section 4.2).

Calibrated ^{14}C ages, together with surface age estimates derived from ^{210}Pb, ^{3}H, ^{39}Ar and the rBC tie-point were used to constrain the D–J model and the COPRA model (see Section 3.4). For the D–J model, the range of H was based on the results of the near-surface dating and topographic maps (see Section 4.3). While this additional constraint is not essential to derive a good fit to the observed ages $t(z)$, the accumulation rate parameter b is sensitive to variations in H. Here, parameter estimates were thus derived from an ensemble of model realizations for the parameter space $\Theta(H, b, h)$ 17.98 m w.e. < H < 31.85 m w.e. (as indicated in Fig. 6), 0 < h < h_{FIT} (with h_{FIT} denoting the height at the firn-ice transition), and for uncertainty range of the dated ages $t(z)$. Realizations were evaluated based on the goodness of fit, i.e., the chi-square of the misfit function (χ^2). For each model realization (N>4000), likelihood weights were assigned according to $L \propto exp\ (-\Delta\chi^2/2)$, where $\Delta\chi^2$ denotes the difference relative to the best fit (minimum misfit). Likelihoods were normalized to unity and used to construct cumulative distributions for each parameter. Parameter estimates, here reported as median values with asymmetric 1σ uncertainties (16th-84th percentile range), are $H = 26^{+5}_{-4}$ m w.e., $h = 6^{+5}_{-3}$ m w.e., and $b = 0.13^{+0.10}_{-0.06}$ m w.e. a^{-1}. The accumulation rate for 1875-1960, b = 0.2 ± 0.1 m w.e. a^{-1}, is consistent with the derived accumulation rate from the cumulative point surface mass balance model (see Fig. 8) prior to significant ablation. We find that the uncertainty in the accumulation rate for Tödi is primarily associated with the probable range in ice thickness and the uncertainty in the strain rate (i.e. h), together contributing approximately 90%, whereas dating uncertainty contributes only about 10%. Overall, the D–J model results in a good fit with the observed ages (for the 1σ range of parameters: χ^2_{red} between 0.13 and 0.21), except for the deepest section where it significantly overestimates the basal age (thriving to infinity near the bed) with the high-resolution in-situ calibrated ^{14}C ages providing crucial information about the basal age of the glacier (Fig. 10). We note that the value estimated for h is lower than expected, with an h/H ratio of around 0.3 compared to the value of 0.8 found by Gabrielli et al. (2026) for another Alpine site (Alto dell'Ortles, Italy). This seems to be consistent with lower ice-flow velocities as expected for a small summit ice cap such as Tödi.

The D-J model assumes steady-state conditions, thus not able to account for variation in accumulation rates. This is reflected by divergence between the ^{14}C dates and the D–J ice flow model, particularly visible for the deepest 1-2 samples (Fig. 10d-e). The COPRA model derives an age scale more closely defined by the actual ^{14}C observations (see Section 3.4), thus accounting for these natural variations and providing a more accurate chronology for the recorded paleo proxies.

https://doi.org/10.5194/egusphere-2026-3356
Preprint. Discussion started: 13 July 2026

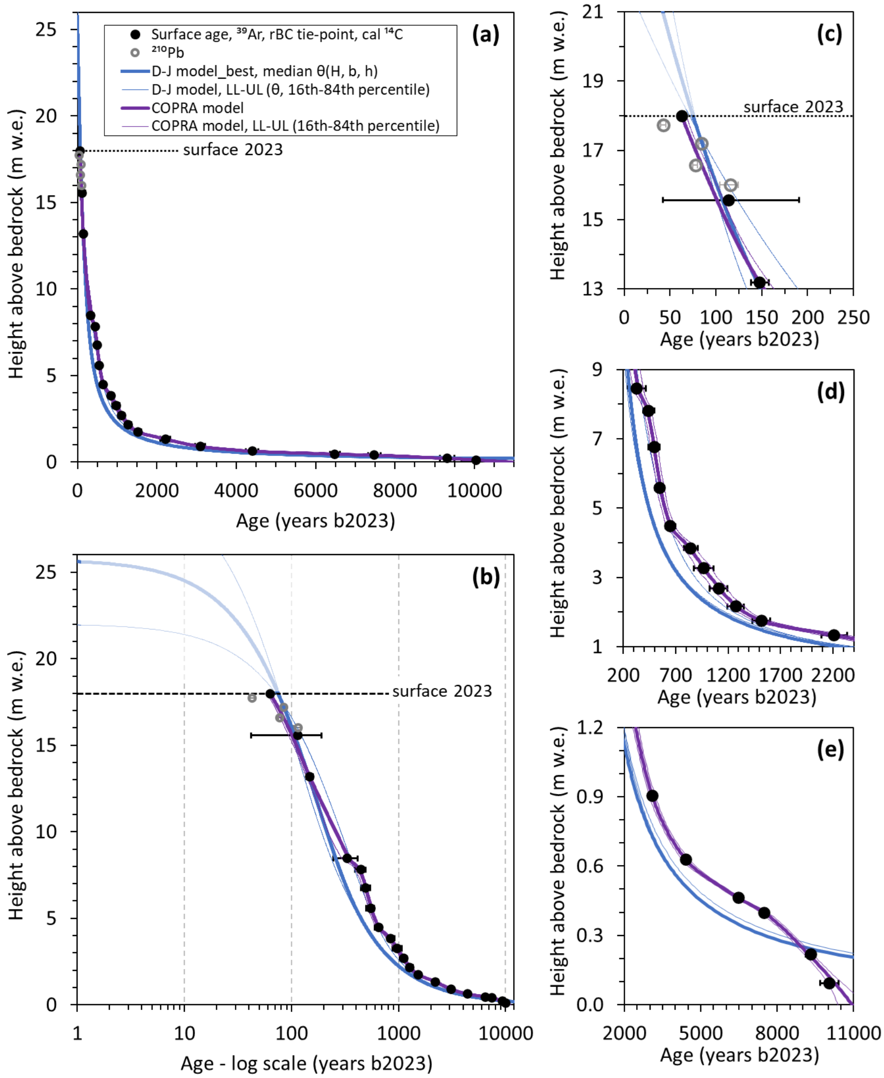

Figure 10. (a) D–J model output (blue) with 1σ confidence band, using calibrated ^{14}C ages together with the surface age (1960), ^{39}Ar and rBC-tie point (black points). COPRA model output (purple) with 1σ confidence band, using the same input data, excluding ^{39}Ar due to its large uncertainty. ^{210}Pb ages are shown for completeness (gray circles). Ages are expressed in years before 2023, and depths are converted to height above bedrock, z (see Supplement S5). (b) Same as panel a, with age on log scale. (c-e) Zoomed sections of panel a.

4.5 Revisiting basal age-altitude relationships in Alpine sites

^{14}C ages from various Alpine ice cores were compiled to compare basal ice ages across sites and to place the Tödi chronology in a broader context (Fig. 11). The compilation includes data from WSS (Bohleber et al., 2020; Wachs et al., 2026), Ortles (Gabrielli et al., 2016; Gabrielli et al., 2026), CG (Jenk et al., 2009; Sigl et al., 2009), Dôme du Goûter (DDG, Legrand et al., 2025), and Col du Dôme (CDD, Preunkert et al., 2019). Across the Alpine region, the age–depth profiles of high-elevation ice cores show broadly similar trends, with pronounced ice thinning toward the base, compressing several millennia into the lowest meter of ice. Basal ice at Tödi is dated to approximately 10 ka cal BP, representing one of the oldest records. Beyond the

https://doi.org/10.5194/egusphere-2026-3356
Preprint. Discussion started: 13 July 2026

absolute age, the strength of the Tödi record lies in its exceptionally high-resolution ^{14}C sampling with comparatively small uncertainties, providing a level of chronological detail rarely achieved at other summit sites and making Tödi a benchmark for its chronology of the oldest ice in the Alps.

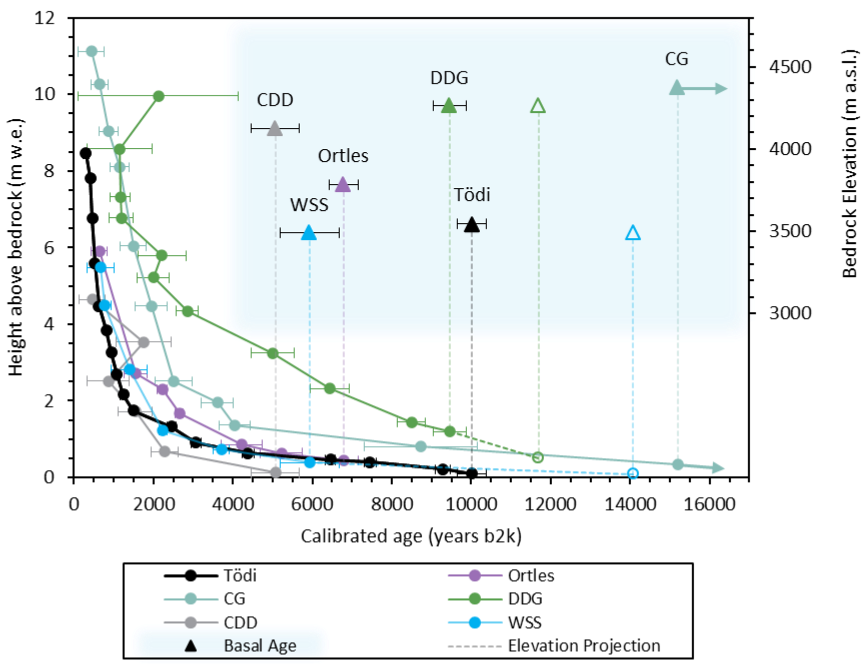

Figure 11. Calibrated ^{14}C ages from Tödi and other investigated Alpine ice cores against height above bedrock (left y-axis, m w.e.). Right y-axis, basal ages extrapolated to bedrock elevation for each site (see Supplement S7). Focusing on the basal ice, only the lowermost ice core sections, all dated by ^{14}C, are shown. CG basal age represents a lower-limit uncertainty and is indicated with an arrow towards older age. Open symbols indicate the following: DDG basal age is not from ^{14}C, but based on δ^{18}O wiggle matching with other paleo-archives; WSS is a previously excluded basal age. Note, lines connecting ^{14}C ages are used for visualization only and are not model fits. (Data from Jenk et al., 2009; Sigl et al., 2009; Gabrielli et al., 2016; Preunkert et al., 2019; Bohleber et al., 2020, Legrand et al., 2025; Gabrielli et al., 2026; Wachs et al., 2026).

Glacier flow dynamics, ice geometry, and englacial temperatures influence vertical strain rates and long-term preservation of old ice. Besides the basal conditions of cold ice frozen to the bed required for the potential to find very old ice, the main factors determining the age of ice close to the bedrock and the shape of the age-depth relationship - as apparent from the equation of the D–J ice flow model - are the ice thickness, the annual accumulation rate and the layer thinning (strain) with depth which depends on the flow velocity. These factors explain part of the discrepancy of the age-depth relationships between the different sites - e.g. the offset between Tödi and DDG by the greater thickness of the latter while the accumulation rates are in the same range. However, we attribute a substantial part of the differences in reported basal ages to methodological factors. To access basal ice, the ice core obviously must have reached bedrock. Because several thousand years may be compressed into the lowest meter of ice, incomplete recovery can underestimate the basal age substantially. Unlike for Tödi where we have strong evidence that bedrock was reached (Section 3.1), solid confirmation is not always available. We hypothesize that the younger basal ages reported from Col du Dôme may reflect incomplete recovery rather than the absence of older ice considering the cold basal temperatures (−11 °C) observed at this site (Vincent et al., 2007a). This is based on the fact that the ^{14}C ages are from the 124 m long 2004 CDK core, reported to be drilled virtually at the same spot as the 1994 C10 core, which reached 126

https://doi.org/10.5194/egusphere-2026-3356
Preprint. Discussion started: 13 July 2026

m depth (Legrand et al., 2013; Preunkert et al., 2019). With no change in ice thickness observed between 1905 and 2005 (Vincent et al., 2007b), an assumed additional 2 m (1.8 m w.e.) of ice below the ^{14}C-dated core would accordingly lift the CDD curve in Figure 11, resulting in close overlay with the curves from Ortles and CG. In other cases, where bedrock was reached, a limited sampling resolution may have biased the apparent basal age toward younger values. This factor is illustrated by the higher sampling density in the deepest 1 m w.e. at Tödi (n = 6) compared to Ortles (n = 2), questioning the reported basal age of the latter (Gabrielli et al., 2016). For WSS, it is important to note that an additional ^{14}C age of ~14 ka cal BP from the very base was excluded from the discussion of the basal age (Bohleber et al., 2020). This was explained by the sample's high dust content potentially resulting in a bias towards older age (related to an analytical challenge for complete removal of carbonates depleted in ^{14}C). While questioning whether the result of such a sample is reliable, obviously an age for the basal ice is then missing, which should somehow be accounted for. Such a potential carbonate bias was estimated in later work with up to around 20% of the calibrated age (Fang et al., 2021). The previously reported result for this lowest sample from WSS (see Bohleber et al., 2020) is included in Figure 11 for completeness (no correction for the potential bias applied).

The surface ages of Tödi and WSS differ markedly, with ~60 years on Tödi compared to ~400 years on WSS (Wachs et al., 2026), indicating distinct long-term mass balance regimes. Different accumulation rates, b, were estimated for Tödi and WSS, with around 0.1 – 0.2 m w.e. a^{-1} and 0.4 – 0.6 m w.e. a^{-1} (Wachs et al., 2026), respectively, which we believe to mainly be caused by differences in the approaches for determination (see Supplement S8). Despite these differences in surface age and accumulation, Tödi and WSS display strikingly consistent age-depth structures and basal thinning behavior. This suggests that summit glaciers near 3500 m a.s.l. may preserve basal ice older than the initially predicted estimate of ~6000 years based on the WSS results (Bohleber et al., 2020). Furthermore, our comparison demonstrates that summit elevation alone is insufficient to reliably predict basal ice age in Alpine glaciers. Therefore, inferring the timing of Neoglaciation or Holocene ice-free conditions requires careful consideration of methodological limitations and site-specific glacier dynamics.

5 Conclusions

The glaciological setting of Tödi closely matches the conceptual framework proposed by Haeberli et al. (2004), who identified cold, wind-exposed, low-accumulation summit glaciers as prime candidates for preserving very old ice. The Tödi summit ice core preserves basal ice dated to ~10 ka cal BP, exceeding the age predicted for this elevation by existing Alpine age–altitude relationships. These results are supported by an exceptionally robust and internally consistent high-resolution radiocarbon chronology, providing direct age control across the deepest section of the core and allowing the stratigraphic integrity of the basal sequence to be assessed with high confidence. The absence of a persistent firn layer and recent negative mass balance decouple the present ice surface from the year of drilling. Multi-tracer surface dating constrains the timing and magnitude of recent thinning, narrowing the surface age to approximately 1960, with an estimated ablation of around 6 m w.e. (~8 m) between 1960 and 2023, consistent with independent mass balance and ice flow model estimates. Together, these observations establish a coherent chronology spanning the entire core and demonstrate that elevation alone is insufficient to predict basal ice age in the Alps, even for cold-based glaciers. Instead, long-term ice preservation is controlled by local glaciological and topographic boundary conditions.

Tödi demonstrates that a compact, wind-exposed, cold-based summit glacier can preserve early Holocene ice despite recent warming and surface lowering. More broadly, the Tödi chronology refines the empirical basis for understanding ice coverage at altitude. Other high-elevation sites with similar geometric and thermal characteristics may preserve older basal ice than currently inferred. Given ongoing thinning in Alpine accumulation areas, establishing robust chronologies that constrain both surface and basal ages is essential for assessing glacier persistence during the Holocene and for placing current ice loss in a longer-term context.

Code and data availability

No custom code was developed in this study. All data used are provided in figures and tables in this paper (see also supplementary information). Previously published data sources are cited throughout the manuscript.

Supplement link

The link to the supplement will be included by Copernicus.

Author contributions

MW wrote the manuscript with contributions from TMJ and MH. MW performed the ^{14}C measurements and the analysis of ^{14}C, ^{3}H, and ^{210}Pb data. SZ contributed to the ^{14}C measurements and analysis. TMJ performed the ^{210}Pb measurements and supervised the analysis of ^{14}C, ^{3}H, and ^{210}Pb data. DW performed the ^{39}Ar measurements and analysis. AE and SB performed the rBC measurements. RM performed the GPR and snow-stake measurements and their analysis. MW, TMJ, and RM planned and participated in the fieldwork, performing ice-core drilling, borehole-temperature measurements, the GPR survey, and snow-stake measurements. MW integrated the different datasets. MW, TMJ, and MH performed the modelling. MW, TMJ, and MS interpreted the synthesized results. TMJ conceived the project and acquired the funding. All authors contributed to the discussion of results and reviewed the manuscript.

Competing interests

The authors declare that there are no competing interests.

Acknowledgements

We thank Giovanni Baccolo (Roma Tre University) for his assistance with ice drilling and ice cutting, as well as Sandra Camara Brügger and Julia Hasler (University of Basel) for their support of ice cutting. We acknowledge Inge Stockinger and Patricia Kramer (Paul Scherrer Institute) for their assistance with ^{210}Pb and ^{3}H measurements, respectively. We thank Barthélémy Anhorn (ETH Zürich) for GPR processing. We thank Tiberiu Sava, Michael Staub, Thomas Laemmel, and Jan Strahl (University of Bern) for supporting ^{14}C measurements. We acknowledge Werner Aeschbach and Markus K. Oberthaler (Heidelberg University) for their support of the project and the provision of ^{39}Ar measurements. Furthermore, Linus Langenbacher, Florian Meienburg, Alexander Junkermann, and Niclas Mandaric for their support during the gas extraction and ATTA measurements. We also thank Martin Lüthi (University of Zürich) for the thermistor chain and Fridolin Walcher for photographs of the Tödi massif. We thank Hans Rauner (mountain guide) and the municipality of Glarus Süd for a safe and successful field campaign on Tödi.

Financial support

This work was supported by the Swiss National Science Foundation (SNFS) under grant number 204845.

https://doi.org/10.5194/egusphere-2026-3356
Preprint. Discussion started: 13 July 2026

References

Agrios, K., Salazar, G., Zhang, Y.-L., Uglietti, C., Battaglia, M., Luginbühl, M., Ciobanu, V. G., Vonwiller, M., and Szidat, S.: Online coupling of pure O2 thermo-optical methods – 14C AMS for source apportionment of carbonaceous aerosols, Nuclear Instruments and Methods in Physics Research Section B: Beam Interactions with Materials and Atoms, 361, 288-293, 2015.

Bohleber, P., Schwikowski, M., Stocker-Waldhuber, M., Fang, L., and Fischer, A.: New glacier evidence for ice-free summits during the life of the Tyrolean Iceman, Scientific Reports, 10, 20513, 2020.

Breitenbach, S. F. M., Rehfeld, K., Goswami, B., Baldini, J. U. L., Ridley, H. E., Kennett, D. J., Prufer, K. M., Aquino, V. V., Asmerom, Y., Polyak, V. J., Cheng, H., Kurths, J., and Marwan, N.: COnstructing Proxy Records from Age models (COPRA), Clim. Past, 8, 1765-1779, 2012.

Carturan, L., De Blasi, F., Dinale, R., Dragà, G., Gabrielli, P., Mair, V., Seppi, R., Tonidandel, D., Zanoner, T., Zendrini, T. L., and Dalla Fontana, G.: Modern air, englacial and permafrost temperatures at high altitude on Mt Ortles (3905 m a.s.l.), in the eastern European Alps, Earth Syst. Sci. Data, 15, 4661-4688, 2023.

Chen, J.: Nuclear Data Sheets for A=39, Nuclear Data Sheets, 149, 1-251, 2018.

Dansgaard, W. and Johnsen, S. J.: A Flow Model and a Time Scale for the Ice Core from Camp Century, Greenland, Journal of Glaciology, 8, 215-223, 1969.

Dyonisius, M. N. and Jenk, T. M.: Ice core methods: Studies of radiocarbon in ice. In: Encyclopedia of Quaternary Science (Third edition), Elias, S. (Ed.), Elsevier, Oxford, 2025.

Eichler, A., Schwikowski, M., Gäggeler, H. W., Furrer, V., Synal, H.-A., Beer, J., Saurer, M., and Funk, M.: Glaciochemical dating of an ice core from upper Grenzgletscher (4200 m a.s.l.), Journal of Glaciology, 46, 507-515, 2000.

Eidevåg, T., Thomson, E. S., Kallin, D., Casselgren, J., and Rasmuson, A.: Angle of repose of snow: An experimental study on cohesive properties, Cold Regions Science and Technology, 194, 103470, 2022.

Fang, L., Jenk, T. M., Singer, T., Hou, S., and Schwikowski, M.: Radiocarbon dating of alpine ice cores with the dissolved organic carbon (DOC) fraction, The Cryosphere, 15, 1537-1550, 2021.

Fang, L., Jenk, T. M., Winski, D., Kreutz, K., Brooks, H. L., Erwin, E., Osterberg, E., Campbell, S., Wake, C., and Schwikowski, M.: Early Holocene ice on the Begguya plateau (Mt. Hunter, Alaska) revealed by ice core 14C age constraints, The Cryosphere, 17, 4007-4020, 2023.

Federal Office of Topography, swisstopo: Tödi, Blatt 1193, Landeskarte der Schweiz 1:25,000, Federal Office of Topography swisstopo, Wabern, Switzerland, 1963.

Federal Office of Topography, swisstopo: Tödi, Blatt 1193, Landeskarte der Schweiz 1:25,000, Federal Office of Topography swisstopo, Wabern, Switzerland, 1997.

Federal Office of Topography, swisstopo: Tödi, Blatt 1193, Landeskarte der Schweiz 1:25,000, Federal Office of Topography swisstopo, Wabern, Switzerland, 2016.

Federal Office of Topography, swisstopo: Tödi, Blatt 1193, Landeskarte der Schweiz 1:25,000, Federal Office of Topography swisstopo, Wabern, Switzerland, 2023.

Fischer, A., Stocker-Waldhuber, M., Frey, M., and Bohleber, P.: Contemporary mass balance on a cold Eastern Alpine ice cap as a potential link to the Holocene climate, Scientific Reports, 12, 1331, 2022.

FOEN: Map of potential permafrost distribution. Federal Office for the Environment (FOEN), Bern, Switzerland, 2005.

Gabrielli, P., Barbante, C., Bertagna, G., Bertó, M., Binder, D., Carton, A., Carturan, L., Cazorzi, F., Cozzi, G., Dalla Fontana, G., Davis, M., De Blasi, F., Dinale, R., Dragà, G., Dreossi, G., Festi, D., Frezzotti, M., Gabrieli, J., Galos, S. P., Ginot, P., Heidenwolf, P., Jenk, T. M., Kehrwald, N., Kenny, D., Magand, O., Mair, V., Mikhalenko, V., Lin, P. N., Oeggl, K., Piffer, G., Rinaldi, M., Schotterer, U., Schwikowski, M., Seppi, R., Spolaor, A., Stenni, B., Tonidandel, D., Uglietti, C., Zagorodnov,

https://doi.org/10.5194/egusphere-2026-3356
Preprint. Discussion started: 13 July 2026

V., Zanoner, T., and Zennaro, P.: Age of the Mt. Ortles ice cores, the Tyrolean Iceman and glaciation of the highest summit of South Tyrol since the Northern Hemisphere Climatic Optimum, The Cryosphere, 10, 2779-2797, 2016.

Gabrielli, P., Jenk, T. M., Bertó, M., Dreossi, G., Festi, D., Kofler, W., Winstrup, M., Oeggl, K., Schwikowski, M., Stenni, B., and Barbante, C.: A multimillennial Alpine ice core chronology synchronized with an accurately dated Arctic Pb record, EGUsphere, 2026, 1-24, 2026.

Gäggeler, H., von Gunten, H. R., Rössler, E., Oeschger, H., and Schotterer, U.: 210Pb-Dating of Cold Alpine Firn/Ice Cores From Colle Gnifetti, Switzerland, Journal of Glaciology, 29, 165-177, 1983.

Gäggeler, H. W., Tobler, L., Schwikowski, M., and Jenk, T. M.: Application of the radionuclide 210Pb in glaciology – an overview, Journal of Glaciology, 66, 447-456, 2020.

Ginot, P., Stampfli, F., Stampfli, D., Schwikowski, M., and Gaeggeler, H.: FELICS, a new ice core drilling system for high-altitude glaciers, Fifth International Workshop on Ice Drilling Technology, Special Issue 56, 38-48, 2002.

GLAMOS: Swiss Glacier Volume Change, release 2025, Glacier Monitoring Switzerland, doi:10.18750/volumechange.2025.r2025, 2025a.

GLAMOS: Swiss Glacier Mass Balance, release 2025. Glacier Monitoring Switzerland, 2025b.

GLAMOS: Swiss Glacier Bulletin 2025. Huss, M., Bauder, A., Barandun, M., Hodel, E., and Linsbauer, A. (eds.). Annual report No. 146, 26 pp., doi:10.18752/glbulletin_2025, 2026.

Guillet, G. and Ravanel, L.: Variations in surface area of six ice aprons in the Mont-Blanc massif since the Little Ice Age, Journal of Glaciology, 66, 777-789, 2020.

Haeberli, W., Gäggeler, H., Baltensperger, U., Jost, D., and Schotterer, U.: The Signal from the Chernobyl Accident in High-Altitude Firn Areas of the Swiss Alps, Annals of Glaciology, 10, 48-51, 1988.

Haeberli, W., Frauenfelder, R., Kääb, A., and Wagner, S.: Characteristics and potential climatic significance of "miniature ice caps" (crest- and cornice-type low-altitude ice archives), Journal of Glaciology, 50, 129-136, 2004.

Henz, A., Reinthaler, J., Nussbaumer, S. U., Leger, T. P. M., Kamleitner, S., Jouvet, G., and Vieli, A.: Alps-wide high-resolution 3D modelling reconstruction of glacier geometry and climatic conditions for the Little Ice Age, The Cryosphere, 19, 5913-5937, 2025.

Herron, M. M. and Langway, C. C.: Firn Densification: An Empirical Model, Journal of Glaciology, 25, 373-385, 1980.

Hou, S., Jenk, T. M., Jiang, W., Zhang, W., Hu, H., Feng, X., Li, H., Wu, S.-Y., Pang, H., Yu, J., Huang, R., Lu, Z.-T., Yang, G.-M., Bender, M., and Schwikowski, M.: A radiometric timescale challenges the chronology of the iconic 1992 Guliya ice core, Science Advances, 11, eadx8837, 2025.

Huber, C. J., Eichler, A., Mattea, E., Brütsch, S., Jenk, T. M., Gabrieli, J., Barbante, C., and Schwikowski, M.: High-altitude glacier archives lost due to climate change-related melting, Nature Geoscience, 17, 110-113, 2024.

Huss, M., Funk, M., and Ohmura, A.: Strong Alpine glacier melt in the 1940s due to enhanced solar radiation, Geophysical Research Letters, 36, 2009.

Huss, M.: Density assumptions for converting geodetic glacier volume change to mass change, The Cryosphere, 7, 877-887, 2013.

Huss, M., Bauder, A., Linsbauer, A., Gabbi, J., Kappenberger, G., Steinegger, U., and Farinotti, D.: More than a century of direct glacier mass-balance observations on Claridenfirn, Switzerland, Journal of Glaciology, 67, 697-713, 2021.

Ivy-Ochs, S., Kerschner, H., Reuther, A., Preusser, F., Heine, K., Maisch, M., Kubik, P. W., and Schlüchter, C.: Chronology of the last glacial cycle in the European Alps, Journal of Quaternary Science, 23, 559-573, 2008.

Jenk, T. M., Szidat, S., Schwikowski, M., Gäggeler, H. W., Brütsch, S., Wacker, L., Synal, H. A., and Saurer, M.: Radiocarbon analysis in an Alpine ice core: record of anthropogenic and biogenic contributions to carbonaceous aerosols in the past (1650-1940), Atmos. Chem. Phys., 6, 5381-5390, 2006.

https://doi.org/10.5194/egusphere-2026-3356
Preprint. Discussion started: 13 July 2026

Jenk, T. M., Szidat, S., Schwikowski, M., Gäggeler, H. W., Wacker, L., Synal, H. A., and Saurer, M.: Microgram level radiocarbon (14C) determination on carbonaceous particles in ice, Nuclear Instruments and Methods in Physics Research Section B: Beam Interactions with Materials and Atoms, 259, 518-525, 2007.

Jenk, T. M., Szidat, S., Bolius, D., Sigl, M., Gäggeler, H. W., Wacker, L., Ruff, M., Barbante, C., Boutron, C. F., and Schwikowski, M.: A novel radiocarbon dating technique applied to an ice core from the Alps indicating late Pleistocene ages, Journal of Geophysical Research: Atmospheres, 114, 2009.

Jouvet, G., Cohen, D., Russo, E., Buzan, J., Raible, C. C., Haeberli, W., Kamleitner, S., Ivy-Ochs, S., Imhof, M. A., Becker, J. K., Landgraf, A., and Fischer, U. H.: Coupled climate-glacier modelling of the last glaciation in the Alps, Journal of Glaciology, 69, 1956-1970, 2023.

Karger, D. N., Nobis, M. P., Normand, S., Graham, C. H., and Zimmermann, N. E.: CHELSA-TraCE21k – high-resolution (1 km) downscaled transient temperature and precipitation data since the Last Glacial Maximum, Clim. Past, 19, 439-456, 2023.

Le Roy, M., Ivy-Ochs, S., Nicolussi, K., Monegato, G., Reitner, J. M., Colucci, R. R., Ribolini, A., Spagnolo, M., and Stoffel, M.: Chapter 20 - Holocene glacier variations in the Alps. In: European Glacial Landscapes, Palacios, D., Hughes, P. D., Jomelli, V., and Tanarro, L. M. (Eds.), Elsevier, 2024.

Legrand, M., Preunkert, S., May, B., Guilhermet, J., Hoffman, H., and Wagenbach, D.: Major 20th century changes of the content and chemical speciation of organic carbon archived in Alpine ice cores: Implications for the long-term change of organic aerosol over Europe, Journal of Geophysical Research: Atmospheres, 118, 3879-3890, 2013.

Legrand, M., McConnell, J. R., Preunkert, S., Wachs, D., Chellman, N. J., Rehfeld, K., Bergametti, G., Wensman, S. M., Aeschbach, W., Oberthaler, M. K., and Friedrich, R.: Alpine ice core record of large changes in dust, sea-salt, and biogenic aerosol over Europe during deglaciation, PNAS Nexus, 4, 2025.

Leuenberger, M. and Flückiger, E.: Research at Jungfraujoch, Science of The Total Environment, 391, 169-176, 2008.

Osmont, D., Wendl, I. A., Schmidely, L., Sigl, M., Vega, C. P., Isaksson, E., and Schwikowski, M.: An 800-year high-resolution black carbon ice core record from Lomonosovfonna, Svalbard, Atmos. Chem. Phys., 18, 12777-12795, 2018.

Preunkert, S., McConnell, J. R., Hoffmann, H., Legrand, M., Wilson, A. I., Eckhardt, S., Stohl, A., Chellman, N. J., Arienzo, M. M., and Friedrich, R.: Lead and Antimony in Basal Ice From Col du Dome (French Alps) Dated With Radiocarbon: A Record of Pollution During Antiquity, Geophysical Research Letters, 46, 4953-4961, 2019.

Ramsey, C. B.: Radiocarbon Calibration and Analysis of Stratigraphy: The OxCal Program, Radiocarbon, 37, 425-430, 1995.

Ramsey, C. B.: Deposition models for chronological records, Quaternary Science Reviews, 27, 42-60, 2008.

Ramsey, C. B.: Bayesian Analysis of Radiocarbon Dates, Radiocarbon, 51, 337-360, 2009.

Ramsey, C. B.: OxCal 4.4.4 calibration program [software]. https://c14.arch.ox.ac.uk/oxcal.html, 2021.

Rasmussen, S. O., Andersen, K. K., Svensson, A. M., Steffensen, J. P., Vinther, B. M., Clausen, H. B., Siggaard-Andersen, M.-L., Johnsen, S. J., Larsen, L. B., Dahl-Jensen, D., Bigler, M., Röthlisberger, R., Fischer, H., Goto-Azuma, K., Hansson, M. E., and Ruth, U.: A new Greenland ice core chronology for the last glacial termination, Journal of Geophysical Research: Atmospheres, 111, 2006.

Reimer, P. J., Austin, W. E. N., Bard, E., Bayliss, A., Blackwell, P. G., Bronk Ramsey, C., Butzin, M., Cheng, H., Edwards, R. L., Friedrich, M., Grootes, P. M., Guilderson, T. P., Hajdas, I., Heaton, T. J., Hogg, A. G., Hughen, K. A., Kromer, B., Manning, S. W., Muscheler, R., Palmer, J. G., Pearson, C., van der Plicht, J., Reimer, R. W., Richards, D. A., Scott, E. M., Southon, J. R., Turney, C. S. M., Wacker, L., Adolphi, F., Büntgen, U., Capano, M., Fahrni, S. M., Fogtmann-Schulz, A., Friedrich, R., Köhler, P., Kudsk, S., Miyake, F., Olsen, J., Reinig, F., Sakamoto, M., Sookdeo, A., and Talamo, S.: The IntCal20 Northern Hemisphere Radiocarbon Age Calibration Curve (0–55 cal kBP), Radiocarbon, 62, 725-757, 2020.

https://doi.org/10.5194/egusphere-2026-3356
Preprint. Discussion started: 13 July 2026

Ritterbusch, F., Tian, L., Tong, A.-M., Gu, J.-Q., Jiang, W., Lu, Z.-T., Shao, L., Tang, M.-X., Yang, G.-M., Zhang, M.-J., and Zhao, L.: A Tibetan ice core covering the past 1,300 years radiometrically dated with ³⁹Ar, Proceedings of the National Academy of Sciences, 119, e2200835119, 2022.

Schlüchter, C., Bini, A., Buoncristiani, J. F., Couterrand, S., Ellwanger, D., Felber, M., Florineth, D., Graf, H. R., Keller, O., Kelly, M., and Schoeneich, P.: Die Schweiz während des letzteiszeitlichen Maximums (LGM), 1:500'000, Bundesamt für Landestopografie swisstopo, Wabern, Switzerland, 2009.

Schotterer, U., Schwarz, P., and Rajner, V.: From the prebomb levels to industrial times. A complete tritium record from an alpine ice core and its relevance for environmental studies, Isotope Techniques in the Study of Environmental Change, Int. Atomic Energy Agency, Vienna, 1998.

Sigl, M., Jenk, T. M., Kellerhals, T., Szidat, S., Gäggeler, H. W., Wacker, L., Synal, H. A., Boutron, C., Barbante, C., Gabrieli, J., and Schwikowski, M.: Towards radiocarbon dating of ice cores, Journal of Glaciology, 55, 985-996, 2009.

Sigl, M., Abram, N. J., Gabrieli, J., Jenk, T. M., Osmont, D., and Schwikowski, M.: 19th century glacier retreat in the Alps preceded the emergence of industrial black carbon deposition on high-alpine glaciers, The Cryosphere, 12, 3311-3331, 2018.

Solomina, O. N., Bradley, R. S., Jomelli, V., Geirsdottir, A., Kaufman, D. S., Koch, J., McKay, N. P., Masiokas, M., Miller, G., Nesje, A., Nicolussi, K., Owen, L. A., Putnam, A. E., Wanner, H., Wiles, G., and Yang, B.: Glacier fluctuations during the past 2000 years, Quaternary Science Reviews, 149, 61-90, 2016.

Spagnesi, A., Bohleber, P., Barbaro, E., Feltracco, M., De Blasi, F., Dreossi, G., Stocker-Waldhuber, M., Festi, D., Gabrieli, J., Gambaro, A., Fischer, A., and Barbante, C.: Preservation of chemical and isotopic signatures within the Weißseespitze millennial old ice cap (Eastern Alps), despite the ongoing ice loss, Frontiers in Earth Science, Volume 11 - 2023, 2023.

Synal, H.-A., Stocker, M., and Suter, M.: MICADAS: A new compact radiocarbon AMS system, Nuclear Instruments and Methods in Physics Research Section B: Beam Interactions with Materials and Atoms, 259, 7-13, 2007.

Szidat, S., Salazar, G. A., Vogel, E., Battaglia, M., Wacker, L., Synal, H.-A., and Türler, A.: 14C Analysis and Sample Preparation at the new Bern Laboratory for the Analysis of Radiocarbon with AMS (LARA), Radiocarbon, 56, 561-566, 2014.

Uglietti, C., Zapf, A., Jenk, T. M., Sigl, M., Szidat, S., Salazar, G., and Schwikowski, M.: Radiocarbon dating of glacier ice: overview, optimisation, validation and potential, The Cryosphere, 10, 3091-3105, 2016.

Vincent, C., Le Meur, E., Six, D., Possenti, P., Lefebvre, E., and Funk, M.: Climate warming revealed by englacial temperatures at Col du Dôme (4250 m, Mont Blanc area), Geophysical Research Letters, 34, 2007a.

Vincent, C., Le Meur, E., Six, D., Funk, M., Hoelzle, M., and Preunkert, S.: Very high-elevation Mont Blanc glaciated areas not affected by the 20th century climate change, Journal of Geophysical Research: Atmospheres, 112, 2007b.

Wachs, D., Spagnesi, A., Bohleber, P., Fischer, A., Stocker-Waldhuber, M., Junkermann, A., Kindermann, C., Langenbacher, L., Mandaric, N., Marks, J., Meienburg, F., Jenk, T. M., Oberthaler, M. K., and Aeschbach, W.: A continuous 6000 a age depth relationship for the remainder of the Weißseespitze summit glacier based on 39Ar and 14C dating, Clim. Past, 22, 173-185, 2026.

Wendl, I. A., Menking, J. A., Färber, R., Gysel, M., Kaspari, S. D., Laborde, M. J. G., and Schwikowski, M.: Optimized method for black carbon analysis in ice and snow using the Single Particle Soot Photometer, Atmos. Meas. Tech., 7, 2667-2681, 2014.

Zekollari, H., Huss, M., and Farinotti, D.: Modelling the future evolution of glaciers in the European Alps under the EURO-CORDEX RCM ensemble, The Cryosphere, 13, 1125-1146, 2019.